

River delta morphotypes emerge from multiscale characterization of shorelines

L. Vulis^{1,2}, A. Tejedor^{3,1}, H. Ma^{4,1}, J. H. Nienhuis⁵, C. M. Broaddus¹, J. Brown⁶, D. A. Edmonds⁶,
J. C. Rowland², and E. Foufoula-Georgiou^{1,7}

¹Department of Civil and Environmental Engineering, University of California Irvine,

²Earth and Environmental Sciences Division, Los Alamos National Laboratory

³Department of Science and Engineering, Sorbonne University Abu Dhabi

⁴State Key Laboratory of Hydrosience and Engineering, Tsinghua University

⁵Department of Physical Geography, Utrecht University

⁶Department of Earth and Atmospheric Sciences, Indiana University

⁷Department of Earth System Science, University of California Irvine

Keypoints

1. Three process-informed, geometric, and spectral metrics are introduced to characterize multiscale shoreline features
2. Unsupervised clustering of the shoreline metrics reveals 5 distinct delta morphotypes which correspond to distinct forcings
3. Morphotypes can be robustly estimated from readily available satellite imagery

Abstract

Delta shoreline structure has long been hypothesized to encode information on the relative influence of fluvial, wave, and tidal processes on delta formation and evolution. We introduce here a novel multiscale characterization of shorelines by defining three process-informed morphological metrics. We show that this characterization yields self-emerging classes of morphologically similar deltas, i.e., delta morphotypes, and also predicts the dominant forcing of each morphotype. Then we show that the dominant forcings inferred from shoreline structure generally align with those estimated via relative sediment fluxes, while positing that misalignments arise from spatiotemporal heterogeneity in deltaic sediment fluxes not captured in their estimates. The proposed framework for shoreline characterization advances our quantitative understanding of how shoreline features reflect delta forcings, and may aid in deciphering paleoclimate from images of ancient deposits and projecting delta morphologic response to changes in sediment fluxes.

Plain Language Summary

It has long been posited that the observed diversity in the shapes of river deltas reflects the relative strength of river, wave, and tide forcings acting on the delta. However, rigorous quantification of delta morphology and how it relates to forcing is still lacking. Here we introduce a new multiscale geometric framework which characterizes river delta morphology via measures of its shoreline structure and then use these measures to first separate deltas into morphological classes called morphotypes and second to infer the dominant forcing of each morphotype. We then show that the dominant forcings revealed by delta shoreline structure generally align with quantitative estimates of the relative amount of sediment transported by each forcing, and posit that misalignments may reflect space-time heterogeneities in the sediment transport rates not captured in their estimated values. The proposed framework enables easy and quantifiable delta classification based on readily-available remote sensing images and may yield insight into predicting deltaic geomorphic response to changing forcings.

Introduction:

River deltas are complex ecogeomorphic landscapes which are home to upwards of 300 million people due to their fertile soils and rich ecosystems (Edmonds et al., 2020). Their intricate hydromorphology controls nearshore biogeochemical function (Knights et al., 2020; Zoccarato et al., 2019), connectivity between surface and subsurface hydrogeology and reservoirs (Sawyer et al., 2015), coastal resilience (Hoitink et al., 2020; Tognin et al., 2021), and ecosystem services (Adams et al., 2018). Deltas are particularly vulnerable to climate change due to their low relief, coastal proximity, and large populations (Edmonds et al., 2020; Hoitink et al., 2020). It is therefore critical to understand how sea level rise and changing riverine sediment loads will impact these systems (Chadwick et al., 2020; Nienhuis et al., 2023) and towards this goal, developing a

quantitative framework which links the driving forces forming deltas to delta morphology and function is imperative.

Fifty years ago, Galloway introduced the paradigm that river deltas are shaped by the interplay of progradational riverine forcings and erosional marine (wave and tide) forcings, which has steered subsequent research on river delta evolution (Galloway, 1975; see also e.g. (Ainsworth et al., 2011; Anthony, 2015; Bhattacharya & Giosan, 2003; Nienhuis et al., 2020; Seybold et al., 2007; Syvitski & Saito, 2007). The relative balance of these forcings and the multiple spatio-temporal scales at which they operate result in a stunning degree of variability in shoreline structure and channel network geometry and topology (Fagherazzi et al., 2015; Hoitink et al., 2017; Jerolmack & Swenson, 2007; Konkol et al., 2022; Tejedor et al., 2016, 2017). Rivers act to prograde the delta planform at large scales and increase roughness at fine scales via the growth of mouth bars and distributary channel expansion (Fagherazzi et al., 2015; Wolinsky et al., 2010). Waves generate alongshore transport that diffuse sediment along the shoreline at fine scales but can lead to spits at coarser scales (Ashton & Giosan, 2011) and suppress mouth-bar development (Jerolmack & Swenson, 2007). Tidal forces widen distributary channels and construct headless channels which lack connections to the upstream river, roughening the shoreline at multiple scales (Hoitink et al., 2017; Nienhuis et al., 2018).

Recently, the relative magnitudes of the forcings in the Galloway framework have been quantified via a sediment flux approach (Nienhuis et al., 2020). However, shoreline shape, a crucial ingredient in the qualitative morphological classification originally posed by Galloway (See Table 2; (Galloway, 1975), has not been quantified in a way to differentiate between visually distinct deltas, nor has been shown to have a clear relationship with forcings, e.g. (Baumgardner, 2016). This is in part because analysis of shoreline structure has typically focused on a single length scale using

metrics such as shoreline variability (Straub et al., 2015) roughness or rugosity measures (Baumgardner, 2016; Caldwell & Edmonds, 2014; Geleynse et al., 2012), and shape factors (Lauzon et al., 2019; Nienhuis et al., 2015; Wolinsky et al., 2010). Such metrics do not necessarily measure shoreline structure at process length scales, nor do they capture the multiscale variability caused by the interplay of the three driving forces.

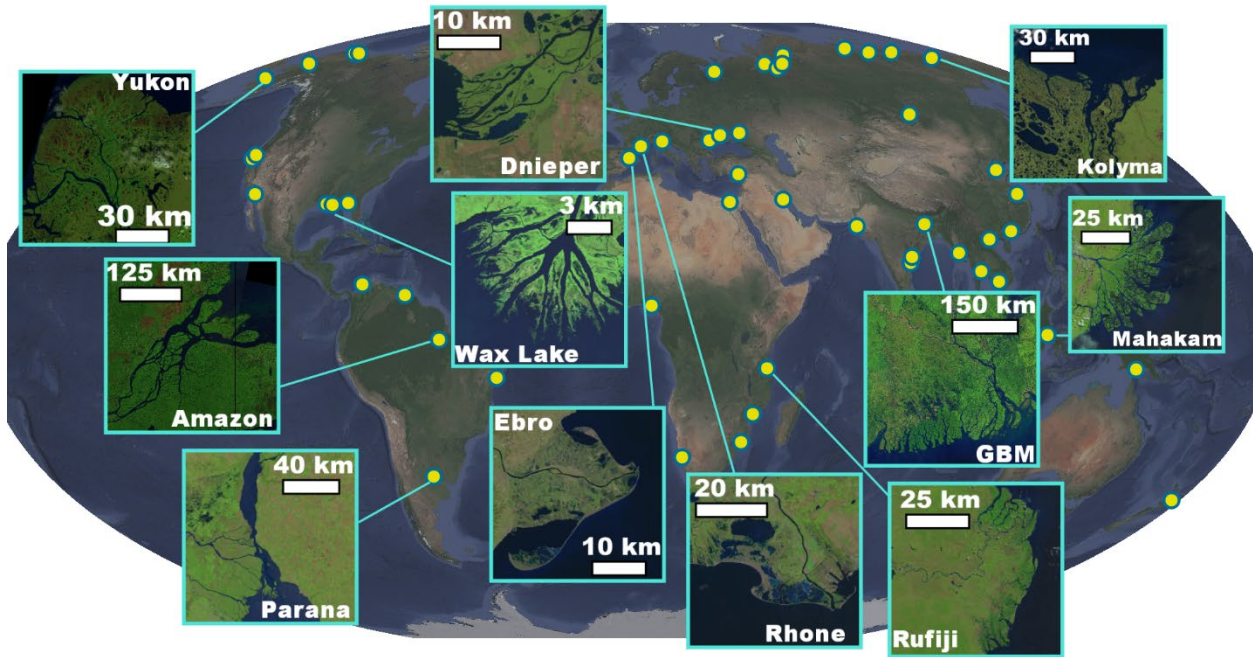


Figure 1. The morphologic variability of Earth's deltas. River deltas show differences in shoreline structure attributed to the relative balance of river, wave, and tidal sediment fluxes (Galloway, 1975). Yellow dots show locations of a globally distributed sample of 54 deltas analyzed in this study. Satellite imagery courtesy of Landsat and Google Earth.

Here, we propose a set of process-informed, multiscale metrics of river delta shoreline shape which combine geometric and spectral measures to develop a quantitative classification of delta morphology. Our approach utilizes localized analysis of shoreline structure both in space and wavenumber domains to isolate features corresponding to different processes acting at multiple scales. Unsupervised clustering of the shoreline morphometrics identifies five classes of

morphologically similar deltas, i.e. delta morphotypes. Based on the values of the process-informed metrics, dominant forcings are attributed to each morphotype, which we then show to generally align with the dominant forcings quantitatively estimated by their relative sediment fluxes (Supplementary Material; Nienhuis et al., 2020). We hypothesize that misalignments between the two are due to spatiotemporal heterogeneity in the sediment fluxes which are not captured by their estimated values. The novel shoreline-based delta morphology classification and comparison to sediment fluxes informs our understanding of how the form and function of these densely populated and biogeochemically rich landscapes might respond to projected changes in sediment fluxes, relative sea level rise, and anthropogenic modification (Chadwick et al., 2020; Edmonds et al., 2020; Hariharan et al., 2022; Hoitink et al., 2020; Moodie & Nittrouer, 2021; Nienhuis et al., 2020; Syvitski & Saito, 2007). It also offers potential application in inferring paleoclimate from ancient delta deposits and interpreting extraterrestrial delta morphology.

Multiscale characterization of delta shorelines

We analyzed the shorelines of 54 river deltas across a range of sizes and a mixture of morphologic features (Supporting Material, Fig. 1; Syvitski & Saito, 2007). River delta shorelines were defined using the Opening Angle Method (OAM) with a critical angle of 45 degrees (Shaw et al., 2008). To define a shoreline, the OAM requires a binary water mask, which was obtained by thresholding water occurrence masks from the Landsat-derived, 30-m spatial resolution Global Surface Water dataset (Pekel et al., 2016).

We defined three scales at which delta shoreline structure exhibits variability, which are linked to the balance of river, tide, and wave forcings: a macroscale (overall delta planform), mesoscale (mouth width scale), and microscale (beach scale). We developed metrics to capture the variability at those scales as discussed below.

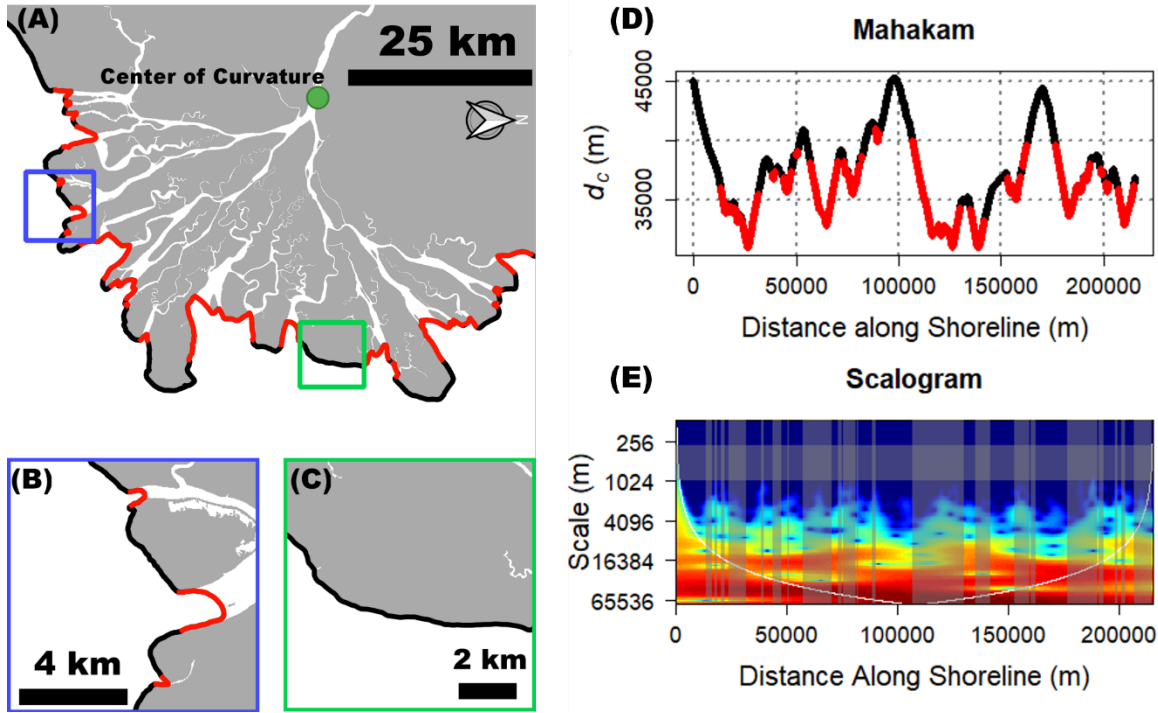


Figure 2. Example of the multiscale features of shoreline structure on the Mahakam Delta, Indonesia. (A) The shoreline of the delta, defined using the Opening Angle Method (OAM) with a critical angle of 45 degrees, shows multiple scales of variability. At the macroscale, a delta may be convex due to river deposition, flat due to wave-driven along shore transport, or concave due to tidal widening and estuarine conditions. This is measured here by the ratio between the radius of curvature and the length of the shoreline. (B) Mouths formed by rivers and tides lead to undulations in the shoreline at a scale determined by the relative river and tide fluxes. (C) At the microscale, waves diffuse sediment parallel to the coast and smooth the shoreline, while rivers and tides roughen it. (D) To measure meso- and microscale variability, the 2D shorelines are mapped to a univariate signal defined as the distance from each point along the shoreline to the center of curvature, $d_c(s)$, where s is the distance along the shoreline. (E) The wavelet transform is used to estimate the fraction of variance contributed by the mouths, fM , marked in red in the preceding panels, and the Gini-corrected Finescale Variance $gFSV$, i.e. the variance from scales (wavelengths) between 300 to 1000 m.

At the macroscale, riverine sediment deposition leads to delta progradation and growth into the receiving basin and generates extrusional shapes (i.e. convex shoreline; Caldwell & Edmonds, 2014; Galloway, 1975). When wave-driven alongshore transport removes the majority of riverine sediment flux, the delta has no protrusion, and is linear (i.e. mostly flat shoreline; Nienhuis et al., 2015). Lastly, tidal forcings erode subaerial sediment into the nearshore and construct a subaqueous platform (Hoitink et al., 2017). This net erosion from land leads to a funnel-shaped, concave subaerial delta, or estuary, which intrudes into the surrounding landscape (i.e. a concave shoreline). We therefore measured the curvature of the entire shoreline (Fig. 2; Jammalamadaka & SenGupta, 2001), to classify deltas as convex (extrusional), concave (intrusional), or flat (see Supporting Material).

At the mesoscale, the influence of rivers, waves, and tides on channel mouths dictates multiple intermediate scales of variability on the shoreline. Tidal forces widen mouths exponentially (Nienhuis et al., 2018) which leads to multiscale undulations in the shoreline (e.g. Amazon and Ganges-Brahmaputra, GBM, delta; Fig. 1). Rivers form mouth bars and bifurcations leading to small but numerous mouths, which result in intermediate to fine scale undulations in the shoreline (e.g. Dnieper delta). Lastly, wave-driven sediment transport prevents mouth bar formation (Jerolmack & Swenson, 2007) and reduces the number of channels (Broaddus et al., 2022), resulting in long shorelines with few, small undulations (e.g. Ebro delta). To measure the contribution of mouths to the overall variability of the shoreline structure, we first projected the shoreline into a univariate spatial-series by recording the distance from each point along the shoreline to the center of curvature of the macroscale shape of the delta (Fig. 2). Then, we identified sections of the shoreline spatial-series corresponding to the mouths and measured via

localized wavelet transforms (Kumar & Foufoula-Georgiou, 1994) the fraction of variance contributed by the mouths, fM (Supporting Material, Fig. 2).

Finally, at the microscale, wave-driven alongshore transport diffuses sediment along the coast and smooths shorelines (Ashton et al., 2001), while rivers and tides introduce variability from distributary and headless channels (Wolinsky et al., 2010). Therefore, we measured the fine scale variance (FSV), as the variance at wavelengths of 300 to 1000 m, to capture these differences (Fig. 2). The lower bound is the result of the minimum reliable scale above which discretization, aliasing, and smoothing effects do not affect the spectra, derived from 30-m spatial resolution Landsat imagery. The upper bound is an approximation of the range of scales within which waves act to smooth shorelines and below which large scale features such as spits begin to emerge. The results are robust to shifting the upper bound from 800 to 1100 m (Supporting Material). Furthermore, to separate shorelines that may have equal fine scale variance but relatively more power at larger wavelengths compared with shorelines that have relatively less power at those wavelengths, the FSV is adjusted by the degree of heterogeneity over the spectral range by multiplying by a spectral Gini coefficient, g , defining the $gFSV$. The spectral Gini coefficient is a measure of the deviation of the spectra from white noise, i.e. a random signal with a flat spectrum (Supporting Material). With these three metrics we quantitatively compare the shoreline morphology of river deltas and explore the possible emergence of distinct morphotypes.

Shoreline morphometric space

The proposed shoreline metrics construct a three-dimensional Shoreline Morphometric Space (SMS) within which deltas can be positioned and compared (Fig. 3). To objectively and robustly identify clusters that categorically classify deltas within this space, we used an unsupervised machine learning algorithm, k-prototypes (a modification of k-means clustering that accounts for

categorical predictors such as the macroscale shape; Huang, 1998). Five morphotypes, i.e., clusters of morphologically similar deltas, emerge from the three-dimensional SMS (Fig. 3) and are displayed in Fig. 4.

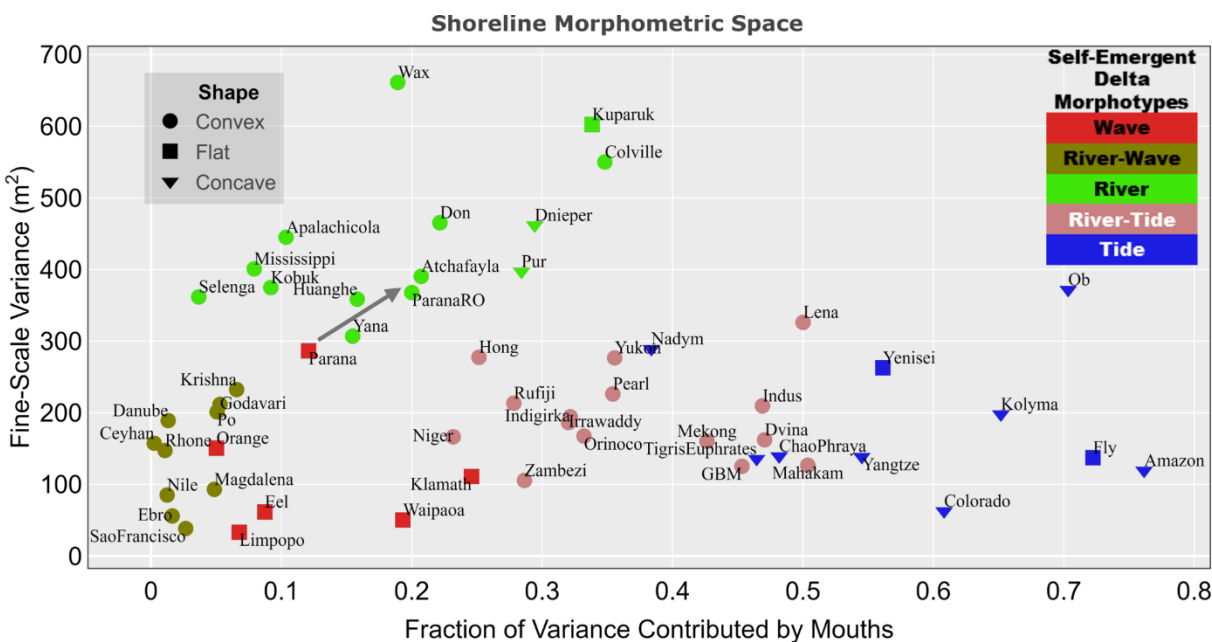


Figure 3. The Shoreline Morphometric Space (SMS). Deltas shorelines are positioned in the three-dimensional space constructed by the macroscale shape, fM , and $gFSV$ metrics. Unsupervised clustering of the SMS using k-prototypes reveals five self-emergent delta morphotypes, i.e. classes of morphologically similar systems. The relative position of the deltas in the SMS elucidates the dominant forcing acting on each morphotype, e.g increased fM a signature of greater tidal influence. The classified deltas are shown in Fig. 4. The arrow indicates the shift in the SMS position of the river distributary section of the Parana shoreline (ParanaRO) compared with the shoreline of the entire Parana, see text for details.

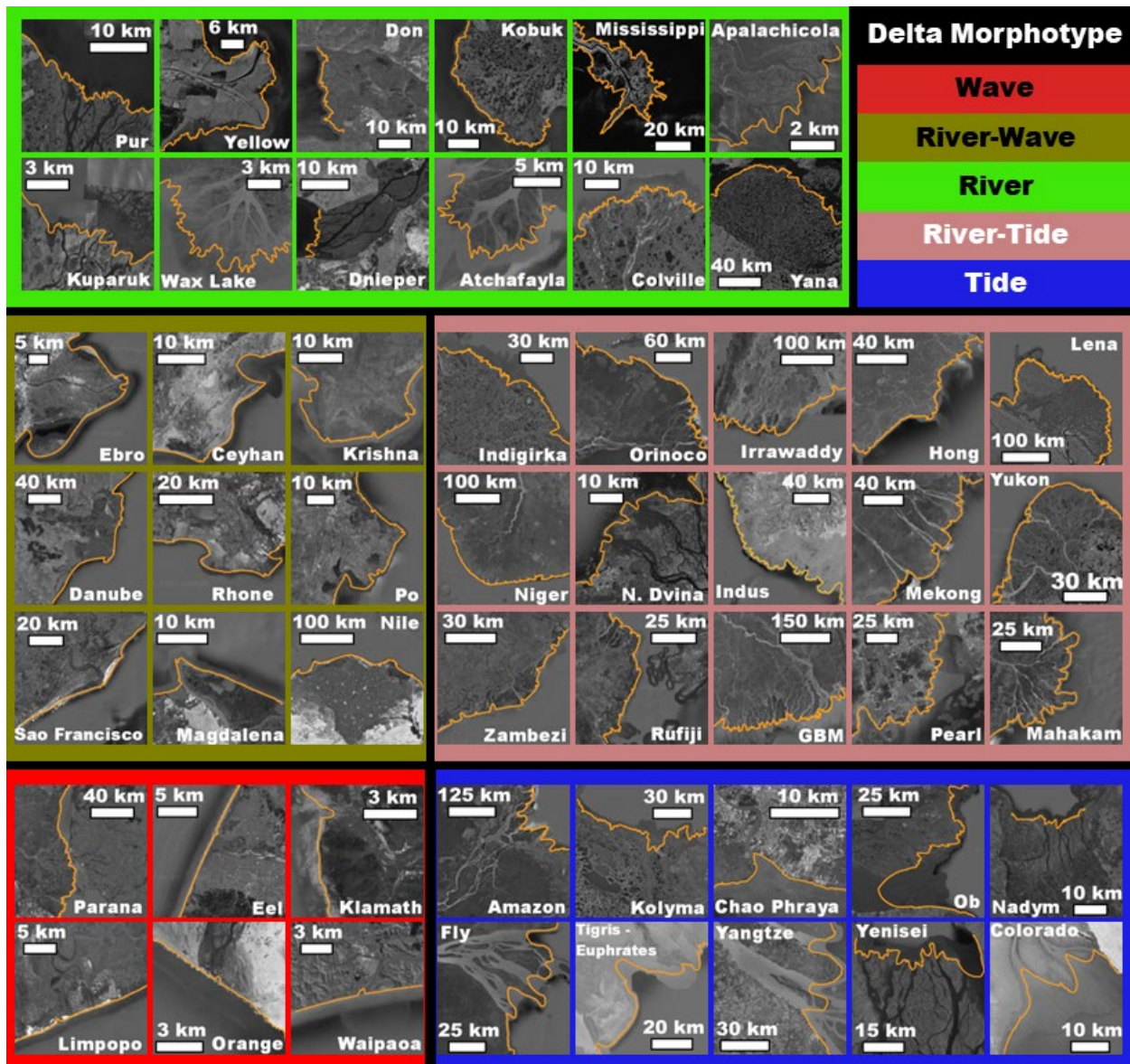


Figure 4. Deltaic morphotypes identified from the SMS. The deltas corresponding to the five morphotypes which emerged from the SMS (Fig. 3). Shorelines are shown in orange with underlying imagery from Landsat or Google Earth.

The first morphotype is denoted as the “tidal morphotype” as these deltas are concave and flat with mouth-dominated shorelines and low finescale variance, indicative of tide-domination (Fig. 4), for example, the Fly and Amazon deltas. It also includes valley-confined deltas like the Ob and

Yenisei due to their wide mouths (Fig. 4). The second morphotype is denoted as the “river morphotype” as these deltas are characterized by an intermediate fraction of variance contributed by mouths, are rough at fine scales, and have a convex planform, for example, the Selenga and Mississippi deltas (Fig. 4). Valley-confined deltas such as the Dnieper and Don, which are concave and flat but have high fine scale variability, are also included as part of the river morphotype. The third morphotype is denoted as the “wave morphotype” as these deltas are flat, lack a subaerial protrusion formed by river deposition, and smooth at fine scales, for example, the Eel and Orange deltas (Fig. 4). The fourth morphotype is denoted as the “river-wave morphotype” as these deltas are convex, smooth at fine scales, typically have spits or flying spits, and little to no variability contributed by mouths, for example, the Ebro and Rhone deltas. Lastly, the fifth morphotype is denoted as the “river-tide morphotype” as it contains convex deltas with tidally widened mouths and headless channels, resulting in intermediate variability contributed by mouths, for example, the Mahakam and Orinoco deltas.

The dominant forcings determined by the quantitative classification of shorelines correspond with expert assessment of the dominant forcings based on qualitative comparisons of delta morphology (Ainsworth et al., 2011; Nienhuis et al., 2020) suggesting that shoreline structure carries a distinct signature of the processes that generated that delta. An interesting further step is to check whether the inferred dominant forcings align with the relative sediment fluxes driven by each forcing, for which we use the recently developed sediment flux estimation framework of Nienhuis et al., (2020).

Are delta morphotypes aligned with relative sediment fluxes?

Each of the 54 deltas was projected onto the ternary Galloway diagram according to the relative sediment flux transported by rivers, waves, and tides as estimated in Nienhuis et al., (2020) (Fig

5). Before contrasting delta morphotypes with their relative sediment fluxes we note a few important issues which we anticipate to cause discrepancies in the mapping between the morphotype and dominant sediment flux. First, the marine sediment fluxes are estimated using simplified, although nonlinear, physical models which transform tidal amplitudes and offshore wave-climate into tidal and wave sediment fluxes, respectively. Therefore, any uncertainty in the tidal amplitude and wave climate will propagate into uncertainty in the sediment flux estimate. Second, sediment fluxes are estimated using single, representative locations for wave climate, tidal amplitude, and fluvial discharge, not acknowledging possible multi-mouth or multi-lobe structure (Nienhuis et al., 2020). Moreover, the sediment fluxes are estimated using contemporary wave climate, tidal amplitude measurements, and modelled, pre-anthropogenically-influenced riverine discharge and sediment loads (Supporting Material; Nienhuis et al., 2020), and represent snapshots of the relative sediment flux, while delta morphology represents the temporally integrated effect of the forcings acting on the delta (Syvitski et al., 2022). Accordingly, any significant spatiotemporal heterogeneity or non-stationarity in the fluxes over each delta's evolution might not be reflected in the contemporary sediment flux estimates. Therefore, some misalignments between delta morphotype and dominant sediment flux are expected, hoping however, that a general agreement will emerge.

The dominant forcings inferred from the delta morphotypes generally align with the estimated relative sediment fluxes driven by each forcing (Fig. 5). For example, the river morphotype and wave morphotype deltas lie in the right corners of the Galloway diagram, and the river-wave morphotype deltas span the space in-between these two end member classes with varying degree of relative tidal influence. Note that deltas in the river morphotype typically have relative river sediment flux more than 80%, although there are notable outliers. A similar observation is made

for deltas in the wave morphotype. Morphological expression of dominance by a single forcing is therefore limited only to small corners of the Galloway space. Morphologically similar deltas which appear scattered or as misalignments between shoreline-inferred dominant forcing and dominant relative sediment flux in the Galloway diagram yield valuable insight into the relationship between observed shoreline structure and the relative sediment fluxes.

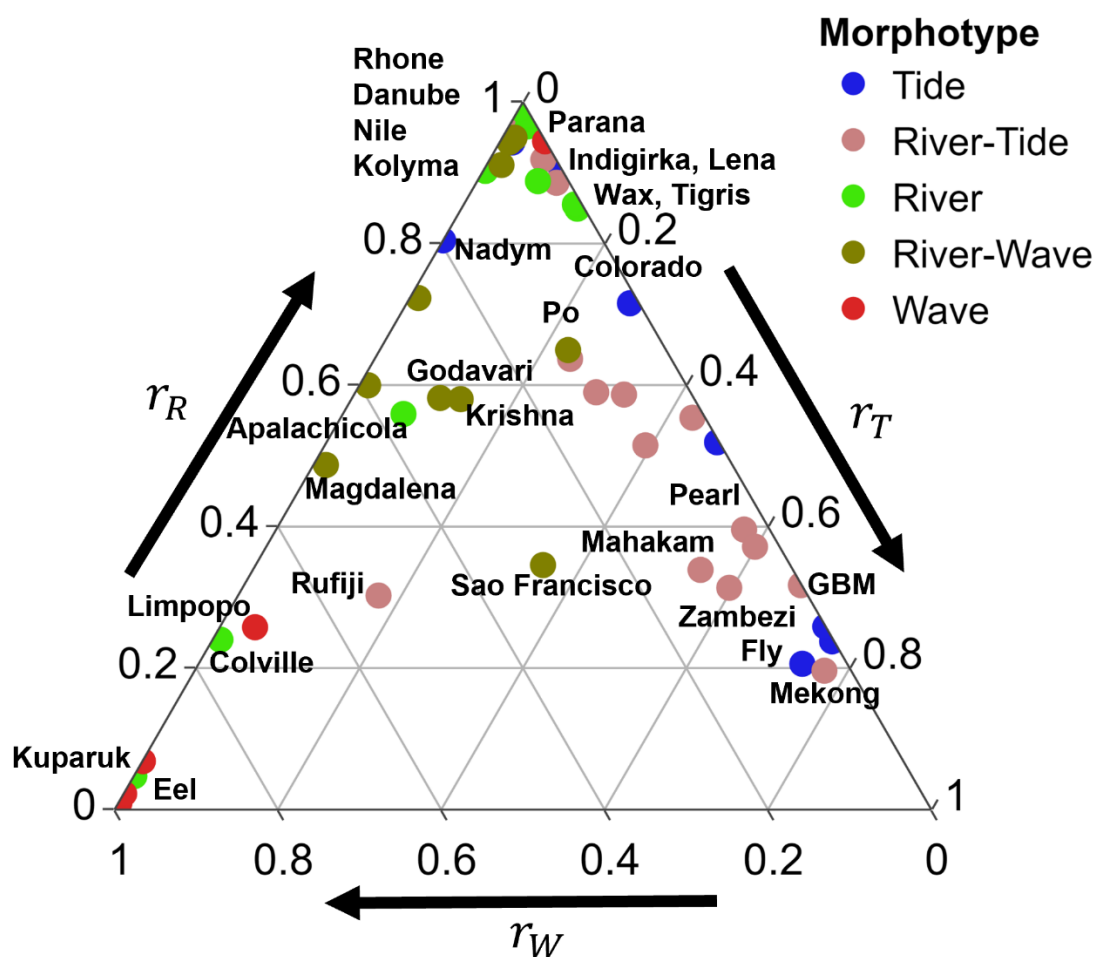


Figure 5. Comparison of delta morphotypes to sediment flux budget. The 54 deltas, colored by their morphotype emergent from the SMS (Fig. 3), are positioned in the Galloway diagram based on their estimated relative sediment fluxes (Nienhuis et al., 2020). Misalignments highlight spatiotemporal heterogeneity in the relative sediment fluxes not captured by their contemporary estimates (see text for discussion).

255 As discussed before, some misalignments arise due to uncertainty in the sediment fluxes estimates.
256 For example, deltas in the tidal morphotype such as the Kolyma and Tigris-Euphrates are assigned
257 relatively low tidal sediment fluxes (Nienhuis et al., 2020), despite displaying clear tidal widening,
258 suggesting under-estimation of the tidal sediment fluxes for these deltas. Similarly, river
259 morphotype deltas such as the Colville, Kuparuk, and Apalachicola, are characterized by abundant
260 mouthbars but have high estimated wave sediment fluxes which are expected to inhibit mouthbar
261 formation (Jerolmack & Swenson, 2007). The Kuparuk and Apalachicola are associated with
262 valley-confined or sheltered shorelines where wave climate data may be particularly uncertain.
263 These misalignments highlight that the shoreline morphometric approach may be more robust than
264 the sediment flux approach for delta classification as it is less sensitive to its defining parameters
265 (e.g. critical angle or range considered for fine scales; see Supporting Material).

266 Further misalignments of interest are the river-tide morphotype deltas and tide morphotype deltas
267 which are scattered across a range of relative tidal influence. This mixture arises as the river-tide
268 and tide morphotypes consist of deltas with intermediate to high fraction of variance contributed
269 by mouths (fM) due to headless and wide channels. However, the river-tide morphotype consists
270 solely of deltas that are convex at the macroscale, e.g. the Irrawaddy, Indus, and Mahakam, which
271 is a signature of historical progradation of the delta planform due to fluvial deposition. Also deltas
272 such as the Zambezi and Rufiji are convex with wide headless channels and have abundant tidal
273 mangroves (Anthony et al., 2021; Erftemeijer & Hamerlynck, 2005), suggesting historical
274 significant river and tidal influence, but have otherwise smooth, sandy shorelines and translating
275 spits indicating recent wave influence. This suggests that although these systems at present have
276 large relative tidal sediment fluxes, the estimated relative sediment fluxes do not capture the

historical river dominance which constructed them. Thus, as tides widen and preserve former distributary channels (Hoitink et al., 2017), and the timescale for waves to erase the convex depositional system formed by river progradation could be on the order of centuries (Nienhuis et al., 2016), the signature of a river remains on its delta long after it has stopped flowing. Therefore, careful consideration must be given to possible temporal heterogeneities in each of the sediment fluxes when computing their relative values and assessing the relationship between morphotype and relative sediment flux (Bhattacharya & Giosan, 2003). This is especially critical for characterizing morphologic response to sediment flux changes, e.g., decreasing riverine sediment delivery or changes in wave climate, and for projecting delta futures under climate change.

Lastly, we hypothesize that some of the misalignments arise because the morphologic metrics are computed along the length of the entire shoreline, although the sediment fluxes are computed via point estimates and don't convey information on spatial heterogeneity in the forcings acting on the delta. For example, the Parana delta lies in the wave morphotype although it has a complex distributary network in its southern half and is dominated by riverine sediment flux (Figs. 3-5). However, the Parana's depositional environment is unique as the Uruguay river runs parallel to its northern shore (Milana & Kröhling, 2015), which we posit acts as a longshore current that smoothens the shoreface but is not captured by the global sediment flux estimation framework which only includes wind-driven longshore transport. To test this hypothesis, we computed the three multiscale metrics of shoreline structure only on the section of the shoreline between the active distributaries in the southern section, terming it ParanaRO, and found that the ParanaRO indeed lies in the river morphotype (Fig. 3), in agreement with its dominant riverine sediment flux (Fig. 5).

Note that the multiscale framework presented herein allows us to further interrogate spatially explicit variability in shoreline structure. In particular, some deltas might exhibit lobes corresponding to distinct morphotypes (e.g. abandoned distributary lobes reworked by marine forces following channel avulsion), shedding further light on the alignment between sediment flux and morphology. However, the framework for estimating sediment fluxes (Nienhuis et al., 2020) will likely need to be adjusted to account for highly spatially variable sediment fluxes given multi-lobe or multi-mouth structures or variable wave climate (Syvitski et al., 2022). We note that combining shoreline metrics with metrics of network complexity (Konkol et al., 2022; Tejedor et al., 2015a, 2015b, 2016, 2017) may help to separate deltas further within the SMS and identify subnetworks that need to be treated separately in terms of their morphology and sediment fluxes. Network information may disaggregate the relatively large river-tide morphotypes and the tide morphotypes, with a possible separation of the valley-confined Ob and Yenisei deltas from estuarine systems such as the Kolyma, Ganges Brahmaputra, and Colorado. This further subdivision of deltas may also be able to yield insight into the influence of other controls on delta morphology including grain size (Caldwell & Edmonds, 2014), valley confinement, cold region processes, or sea level history (Nienhuis et al., 2023; Overeem et al., 2022). Interestingly, no systematic signature of near-shore sea-ice, permafrost, or river-ice was detected on shoreline structure (Lauzon et al., 2019; Overeem et al., 2022; Piliouras et al., 2021), except for a lack of wave influenced Arctic systems which may relate to the short wind fetch present due to sea ice (Barnhart et al., 2014) or the presence of a shallow subaqueous ramp dampening wave runup and breakup at the subaerial shoreline (Overeem et al., 2022).

Conclusion

We have introduced a novel quantitative framework to classify river delta morphology based on a multiscale characterization of delta shoreline structure through geometric and spectral metrics which form a three-dimensional shoreline morphometric space (SMS). Unsupervised classification of 54 deltas projected in the SMS reveals self-emergent morphologically similar deltas, i.e. delta morphotypes which are further associated with dominant forcings based on the metrics. We then found that dominant forcings inferred from shoreline structure generally align with the dominant forcings quantitatively estimated by their relative sediment fluxes. We posit that misalignments arise due to possible spatiotemporal variability in the dominant forcings not captured in the relative sediment fluxes, providing a basis for more detailed analysis of those deltas. The proposed shoreline morphologic classification framework relies on readily available satellite imagery making it easily applicable for remote, poorly instrumented coastlines and basins as well as on extraterrestrial bodies, for which forcings are not available.

Acknowledgements

L.V. was supported by funding from the University of California Lab Fees In Residence Graduate Fellowship Grant L21GF3569, and NASA Earth and Space Science Fellowship Grant 80NSSC18K1409. LV., A.T., H.M., C.B., and E. F-G., were supported by the United Kingdom Research \& Innovation Living Deltas Hub NES0089261. L.V., A.T., H.M., C.B., and E.F-G. were supported by the National Science Foundation through the Collaborative Research program Grant EAR1811909 while D.E., C.B., and J.B. were supported through Collaborative Research program Grant EAR1812019. J.C.R. was supported by the InteRFACE project through the DOE. J.H.N. was supported by the Dutch Research Council through Grant NWO-vi.veni.192.123. We also

344 acknowledge helpful discussion on spectral analyses with Phong V. V. Le and Clement Guilloteau,
345 as well as fruitful discussions with the CSDMS community at large.

346 **Open Research**

347 The values of each metric and relative sediment flux are available in the supplementary material
348 and will be made available via Zenodo for final publication. The Global Surface Water masks used
349 to define the shorelines are available at [https://developers.google.com/earth-](https://developers.google.com/earth-engine/datasets/catalog/JRC_GSW1_1_GlobalSurfaceWater?hl=en)
350 [engine/datasets/catalog/JRC_GSW1_1_GlobalSurfaceWater?hl=en](https://developers.google.com/earth-engine/datasets/catalog/JRC_GSW1_1_GlobalSurfaceWater?hl=en). ROAM, A fast R-based
351 implementation of the Opening Angle Method, is available at <http://github.com/lvulis/ROAM>.

352 **References**

- 353 Adams, H., Adger, W. N., & Nicholls, R. J. (2018). Ecosystem Services Linked to Livelihoods
354 and Well-Being in the Ganges-Brahmaputra-Meghna Delta. In *Ecosystem Services for Well-
355 Being in Deltas* (pp. 29–47). Cham: Springer International Publishing.
356 https://doi.org/10.1007/978-3-319-71093-8_2
- 357 Ainsworth, R. B., Vakarelov, B. K., & Nanson, R. A. (2011). Dynamic spatial and temporal
358 prediction of changes in depositional processes on clastic shorelines: Toward improved
359 subsurface uncertainty reduction and management. *AAPG Bulletin*, 95(2), 267–297.
360 <https://doi.org/10.1306/06301010036>
- 361 Anthony, E. J. (2015). Wave influence in the construction, shaping and destruction of river
362 deltas: A review. *Marine Geology*, 361, 53–78.
363 <https://doi.org/10.1016/j.margeo.2014.12.004>
- 364 Anthony, E. J., Besset, M., Zainescu, F., & Goichot, M. (2021). Geomorphology of a tropical
365 river delta under pressure: the Rufiji delta, Tanzania—context, channel connectivity and
366 alongshore morpho-sedimentary and hydrodynamic variability. *Geo-Marine Letters*, 41(2).
367 <https://doi.org/10.1007/s00367-021-00695-7>
- 368 Ashton, A., & Giosan, L. (2011). Wave-angle control of delta evolution. *Geophysical Research
369 Letters*, 38(13), 1–6. <https://doi.org/10.1029/2011GL047630>
- 370 Ashton, A., Murray, A. B., & Arnoult, O. (2001). Formation of coastline features by large-scale
371 instabilities induced by high-angle waves. *Nature*, 414(6861), 296–300.
372 <https://doi.org/10.1038/35104541>
- 373 Barnhart, K. R., Overeem, I., & Anderson, R. S. (2014). The effect of changing sea ice on the
374 physical vulnerability of Arctic coasts. *Cryosphere*, 8(5), 1777–1799.
375 <https://doi.org/10.5194/tc-8-1777-2014>
- 376 Baumgardner, S. E. (2016). *Quantifying Galloway: Fluvial, Tidal and Wave Influence on
377 Experimental and Field Deltas*.
- 378 Bhattacharya, J. P., & Giosan, L. (2003). Wave-influenced deltas: geomorphological
379 implications for facies reconstruction. *Sedimentology*, 50(1), 187–210.
380 <https://doi.org/10.1046/j.1365-3091.2003.00545.x>
- 381 Broaddus, C. M., Vulis, L. M., Nienhuis, J. H., Tejedor, A., Brown, J., Foufoula-Georgiou, E., &
382 Edmonds, D. A. (2022). First-Order River Delta Morphology Is Explained by the Sediment
383 Flux Balance From Rivers, Waves, and Tides. *Geophysical Research Letters*, 49(22).
384 <https://doi.org/10.1029/2022GL100355>
- 385 Caldwell, R. L., & Edmonds, D. A. (2014). The effects of sediment properties on deltaic
386 processes and morphologies: A numerical modeling study. *Journal of Geophysical
387 Research: Earth Surface*, 119(5), 961–982. <https://doi.org/10.1002/2013JF002965>

388 Chadwick, A. J., Lamb, M. P., & Ganti, V. (2020). Accelerated river avulsion frequency on
389 lowland deltas due to sea-level rise. *Proceedings of the National Academy of Sciences of the*
390 *United States of America*, 117(30), 17584–17590. <https://doi.org/10.1073/pnas.1912351117>

391 Edmonds, D. A., Caldwell, R. L., Brondizio, E. S., & Siani, S. M. O. (2020). Coastal flooding
392 will disproportionately impact people on river deltas. *Nature Communications*, 11(1), 1–8.
393 <https://doi.org/10.1038/s41467-020-18531-4>

394 Erftemeijer, P. L. A., & Hamerlynck, O. (2005). Die-Back of the Mangrove *Heritiera littoralis*
395 Dryand, in the Rufiji Delta (Tanzania) Following El Niño Floods. *Journal of Coastal*
396 *Research*, (42), 228–235. Retrieved from <https://www.jstor.org/stable/25736988>

397 Fagherazzi, S., Edmonds, D. A., Nardin, W., Leonardi, N., Canestrelli, A., Falcini, F., et al.
398 (2015). Dynamics of river mouth deposits. *Reviews of Geophysics*, 53(3), 642–672.
399 <https://doi.org/10.1002/2014RG000451>

400 Galloway, W. E. (1975). Process framework for describing the morphological and stratigraphic
401 evolution of deltaic depositional systems. *Deltas: Models for Exploration*, (September), 87–
402 98.

403 Geleynse, N., Voller, V. R., Paola, C., & Ganti, V. (2012). Characterization of river delta
404 shorelines. *Geophysical Research Letters*, 39(17), 2–7.
405 <https://doi.org/10.1029/2012GL052845>

406 Hariharan, J., Passalacqua, P., Xu, Z., Michael, H. A., Steel, E., Chadwick, A., et al. (2022).
407 Modeling the Dynamic Response of River Deltas to Sea-Level Rise Acceleration. *Journal*
408 *of Geophysical Research: Earth Surface*, 127(9). <https://doi.org/10.1029/2022JF006762>

409 Hoitink, A. J. F., Wang, Z. B., Vermeulen, B., Huismans, Y., & Kästner, K. (2017). Tidal
410 controls on river delta morphology. *Nature Geoscience*, 10(9), 637–645.
411 <https://doi.org/10.1038/ngeo3000>

412 Hoitink, A. J. F., Nittrouer, J. A., Passalacqua, P., Shaw, J. B., Langendoen, E. J., Huismans, Y.,
413 & van Maren, D. S. (2020). Resilience of River Deltas in the Anthropocene. *Journal of*
414 *Geophysical Research: Earth Surface*, 125(3), 1–24. <https://doi.org/10.1029/2019JF005201>

415 Huang, Z. (1998). Extensions to the k-Means Algorithm for Clustering Large Data Sets with
416 Categorical Values. *Data Mining and Knowledge Discovery*, 2(3), 283–304.
417 <https://doi.org/10.1023/A:1009769707641>

418 Jammalamadaka, S. R., & SenGupta, A. (2001). *Topics in Circular Statistics* (Vol. 5). World
419 Scientific. <https://doi.org/10.1142/4031>

420 Jerolmack, D. J., & Swenson, J. B. (2007). Scaling relationships and evolution of distributary
421 networks on wave-influenced deltas. *Geophysical Research Letters*, 34(23), 1–5.
422 <https://doi.org/10.1029/2007GL031823>

- Knights, D., Sawyer, A. H., Barnes, R. T., Piliouras, A., Schwenk, J., Edmonds, D. A., & Brown, A. M. (2020). Nitrate Removal Across Ecogeomorphic Zones in Wax Lake Delta, Louisiana (USA). *Water Resources Research*, 56(8), 1–15. <https://doi.org/10.1029/2019WR026867>
- Konkol, A., Schwenk, J., Katifori, E., & Shaw, J. B. (2022). Interplay of River and Tidal Forcings Promotes Loops in Coastal Channel Networks. *Geophysical Research Letters*, 49(10). <https://doi.org/10.1029/2022GL098284>
- Kumar, P., & Foufoula-Georgiou, E. (1994). *Wavelet Analysis in Geophysics: An Introduction. Wavelet Analysis and Its Applications* (Vol. 4). <https://doi.org/10.1016/B978-0-08-052087-2.50007-4>
- Lauzon, R., Piliouras, A., & Rowland, J. C. (2019). Ice and permafrost effects on delta morphology and channel dynamics. *Geophysical Research Letters*, (May), 2019GL082792. <https://doi.org/10.1029/2019GL082792>
- Milana, J. P., & Kröhling, D. (2015). Climate changes and solar cycles recorded at the Holocene Paraná Delta, and their impact on human population. *Scientific Reports*, 5(August). <https://doi.org/10.1038/srep12851>
- Moodie, A. J., & Nittrouer, J. A. (2021). Optimized river diversion scenarios promote sustainability of urbanized deltas. *Proceedings of the National Academy of Sciences*, 118(27). <https://doi.org/10.1073/pnas.2101649118>
- Nienhuis, J. H., Ashton, A. D., & Giosan, L. (2015). What makes a delta wave-dominated? *Geology*, 43(6), 511–514. <https://doi.org/10.1130/G36518.1>
- Nienhuis, J. H., Ashton, A. D., & Giosan, L. (2016). Littoral steering of deltaic channels. *Earth and Planetary Science Letters*, 453(April 2018), 204–214. <https://doi.org/10.1016/j.epsl.2016.08.018>
- Nienhuis, J. H., Hoitink, A. J. F. T., & Törnqvist, T. E. (2018). Future Change to Tide-Influenced Deltas. *Geophysical Research Letters*, 45(8), 3499–3507. <https://doi.org/10.1029/2018GL077638>
- Nienhuis, J. H., Ashton, A. D., Edmonds, D. A., Hoitink, A. J. F., Kettner, A. J., Rowland, J. C., & Törnqvist, T. E. (2020). Global-scale human impact on delta morphology has led to net land area gain. *Nature*, 577(7791), 514–518. <https://doi.org/10.1038/s41586-019-1905-9>
- Nienhuis, J. H., Kim, W., Milne, G. A., Quock, M., Slangen, A. B. A., & Törnqvist, T. E. (2023). River Deltas and Sea-Level Rise. *Annual Review of Earth and Planetary Sciences*, 51(1). <https://doi.org/10.1146/annurev-earth-031621-093732>
- Overeem, I., Nienhuis, J. H., & Piliouras, A. (2022). Ice-dominated Arctic deltas. *Nature Reviews Earth and Environment*, 3(4), 225–240. <https://doi.org/10.1038/s43017-022-00268-x>

- Pekel, J.-F., Cottam, A., Gorelick, N., & Belward, A. S. (2016). High-resolution mapping of global surface water and its long-term changes. *Nature*, 540(7633), 418–422. <https://doi.org/10.1038/nature20584>
- Piliouras, A., Lauzon, R., & Rowland, J. C. (2021). Unraveling the Combined Effects of Ice and Permafrost on Arctic Delta Morphodynamics. *Journal of Geophysical Research: Earth Surface*, 126(4), 1–17. <https://doi.org/10.1029/2020JF005706>
- Sawyer, A. H., Edmonds, D. A., & Knights, D. (2015). Surface water-groundwater connectivity in deltaic distributary channel networks. *Geophysical Research Letters*, 42(23), 10299–10306. <https://doi.org/10.1002/2015GL066156>
- Seybold, H., Andrade, J. S., & Herrmann, H. J. (2007). Modeling river delta formation. *Proceedings of the National Academy of Sciences of the United States of America*, 104(43), 16804–16809. <https://doi.org/10.1073/pnas.0705265104>
- Shaw, J. B., Wolinsky, M. A., Paola, C., & Voller, V. R. (2008). An image-based method for shoreline mapping on complex coasts. *Geophysical Research Letters*, 35(12), 1–5. <https://doi.org/10.1029/2008GL033963>
- Straub, K. M., Li, Q., & Benson, W. M. (2015). Influence of sediment cohesion on deltaic shoreline dynamics and bulk sediment retention: A laboratory study. *Geophysical Research Letters*, 42(22), 9808–9815. <https://doi.org/10.1002/2015GL066131>
- Syvitski, J., & Saito, Y. (2007). Morphodynamics of deltas under the influence of humans. *Global and Planetary Change*, 57(3–4), 261–282. <https://doi.org/10.1016/j.gloplacha.2006.12.001>
- Syvitski, J., Anthony, E., Saito, Y., Zăinescu, F., Day, J., Bhattacharya, J. P., & Giosan, L. (2022). Large deltas, small deltas: Toward a more rigorous understanding of coastal marine deltas. *Global and Planetary Change*, 218. <https://doi.org/10.1016/j.gloplacha.2022.103958>
- Tejedor, A., Longjas, A., Zaliapin, I., & Foufoula-Georgiou, E. (2015a). Delta channel networks: 1. A graph-theoretic approach for studying connectivity and steady state transport on deltaic surfaces. *Water Resources Research*, 51(6), 3998–4018. <https://doi.org/10.1002/2014WR016577>
- Tejedor, A., Longjas, A., Zaliapin, I., & Foufoula-Georgiou, E. (2015b). Delta channel networks: 2. Metrics of topologic and dynamic complexity for delta comparison, physical inference, and vulnerability assessment. *Water Resources Research*, 51(6), 4019–4045. <https://doi.org/10.1002/2014WR016604>
- Tejedor, A., Longjas, A., Caldwell, R., Edmonds, D. A., Zaliapin, I., & Foufoula-Georgiou, E. (2016). Quantifying the signature of sediment composition on the topologic and dynamic complexity of river delta channel networks and inferences toward delta classification. *Geophysical Research Letters*, 43(7), 3280–3287. <https://doi.org/10.1002/2016GL068210>

- 494 Tejedor, A., Longjas, A., Edmonds, D. A., Zaliapin, I., Georgiou, T. T., Rinaldo, A., &
495 Foufoula-Georgiou, E. (2017). Entropy and optimality in river deltas. *Proceedings of the*
496 *National Academy of Sciences*, 114(44), 11651–11656.
497 <https://doi.org/10.1073/pnas.1708404114>
- 498 Tognin, D., D’Alpaos, A., Marani, M., & Carniello, L. (2021). Marsh resilience to sea-level rise
499 reduced by storm-surge barriers in the Venice Lagoon. *Nature Geoscience*, 14(12), 906–
500 911. <https://doi.org/10.1038/s41561-021-00853-7>
- 501 Wolinsky, M. A., Edmonds, D. A., Martin, J., & Paola, C. (2010). Delta allometry: Growth laws
502 for river deltas. *Geophysical Research Letters*, 37(21), 1–6.
503 <https://doi.org/10.1029/2010GL044592>
- 504 Zoccarato, C., da Lio, C., Tosi, L., & Teatini, P. (2019). A coupled biomorpho-geomechanical
505 model of tidal marsh evolution. *Water Resources Research*, 2019WR024875.
506 <https://doi.org/10.1029/2019WR024875>
- 507